RSC Advances

PAPER

View Article Online
View Journal | View Issue

Cite this: *RSC Adv.*, 2022, **12**, 20096

Selectivity profile comparison for certain γ-butyrolactone and oxazolidinone-based ligands on a sigma 2 receptor over sigma 1: a molecular docking approach†

Richie R. Bhandare, *[ab] Dilep Kumar Sigalapalli,*[c] Afzal B. Shaik, *[c] Daniel J. Canney[d] and Benjamin E. Blass*[d]

Sigma receptors (σ_1 R and σ_2 R) are pharmacologically characterized membrane-bound receptors that bind a wide range of chemical compounds. Alzheimer's disease, traumatic brain injury, schizophrenia, and neuropathic pain have all been associated with abnormal σ_2 activity. The σ_2 receptor has recently been identified as a potential therapeutic target for inhibiting the formation of amyloid plaques. Numerous laboratories are now investigating the potential of σ_2 ligands. Small molecule discovery is the focus of current research, with the goal of using target-based action to treat a variety of illnesses and ailments. Functionalized γ-butyrolactone and oxazolidinone-based ligands, in particular, are pharmacologically important scaffolds in drug discovery research and have been thoroughly examined for σ_2 receptor efficacy. The purpose of this study was to evaluate the pharmacophoric features of different σ_2 receptor ligands using *in silico* techniques. This study used a library of 58 compounds having a γ-butyrolactone and oxazolidinone core. To investigate the binding characteristics of the ligands with the σ_2 receptor, a 3D homology model was developed. To understand the binding pattern of the γ-butyrolactone and oxazolidinone based ligands, molecular docking studies were performed on both σ_1 and σ_2 receptors. Furthermore, MM/GBSA binding energy calculations were used to confirm the binding of ligands on the σ_2 over σ_1 receptor. These *in silico* findings will aid in the discovery of selective σ_2 ligands with good pharmacophoric properties and potency in the future.

Received 6th June 2022
Accepted 4th July 2022

DOI: 10.1039/d2ra03497b

rsc.li/rsc-advances

1. Introduction

In 1976, W. R. Martin *et al.* published the results of a study on the impact of morphine, ketocyclazocine, and (±)-SKF-100047 in dogs with chronic spinal disease. They found that these three compounds elicited distinctly different responses and hypothesized that each was interacting with a different pharmacological target. They labeled these previously unidentified targets as the μ-opioid receptor (morphine type, MOR), the κ-opioid receptor (ketocyclazocine type, KOR), and the σ-opioid receptor (SKF-100047 like).[1] Follow-up studies with the individual enantiomers of SKF-100047 revealed that each isomer interacted with a different biochemical target. (−)-SKF-100047 interacts with MOR and KOR to produce an opioid type response, but (+)-SKF-100047 produces a non-opioid response through the sigma receptor (σR).[2] Eventually, it was determined that there are two subtypes of this receptor, which have been designated as sigma-1 (σ_1) and sigma-2 (σ_2).[3] An X-ray structure of human σ_1 was reported in 2016,[4] but to date there are no known ligands for this receptor.

The true nature of σ_2, however, remained a mystery for nearly 40 years. In 2017, A. C. Kruse *et al.* demonstrated that this receptor is identical to the Transmembrane Protein 97 (TMEM97, also known as MAC30 (Meningioma-associated protein)),[5] and an X-ray structure was published in 2021.[6] Similar to σ_1, there are no known natural functional σ_2 ligands. It has been demonstrated that this protein is present in the endoplasmic reticulum (ER) and lysosomes where it binds to cholesterol, but the pharmacological role of σ_2 has not been determined.[7] Numerous disease states such as schizophrenia,[8] Alzheimer's disease,[9] neuropathic pain,[10] traumatic brain injury,[11] Niemann-Pick disease,[12] and cancer[13] have been linked to σ_2 and this has prompted many research teams to investigate

[a]*College of Pharmacy & Health Sciences, Ajman University, PO Box 340, Ajman, United Arab Emirates. E-mail: r.bhandareh@ajman.ac.ae*

[b]*Center of Medical and Bio-allied Health Sciences Research, Ajman University, Ajman, United Arab Emirates*

[c]*Department of Pharmaceutical Chemistry, Vignan Pharmacy College, Jawaharlal Nehru Technological University, Vadlamudi, 522213, Andhra Pradesh, India. E-mail: dileepsigalapalli@gmail.com; bashafoye@gmail.com*

[d]*Temple University School of Pharmacy, 3307 North Broad Street, Philadelphia, PA 194140, USA. E-mail: benjamin.blass@temple.edu*

† Electronic supplementary information (ESI) available. See https://doi.org/10.1039/d2ra03497b

the potential therapeutic utility of σ_2 ligands. Numerous *in vivo* active σ_2 ligands have been identified and some have reached human clinical trials. UKH-1114 (**1**, σ_2 $K_i = 46$ nM) is efficacious in animal models of pain,[14] while Siramesine (**2**, σ_2 $K_i = 0.12$ nM) is efficacious in animal models of depression and anxiety.[15] The radioligand [^{18}F]ISO-1 (**3**, σ_2 $K_i = 6.9$ nM) has been studied as a possible PET ligand in the treatment of breast cancer,[16] while CT1812 (**4**, σ_2 $K_i = 8.5$ nM) has been the subject of clinical trials as a potential Alzheimer's disease therapy (Fig. 1).[17]

Recently, we reported our discovery of two novel classes of σ_2 ligands, oxazolidin-2-ones (**5**) and functionalized γ-butyrolactones (**6**).[18–20] The synthetic protocol for the synthesis of these two classes of compounds is outlined in the ESI† (Schemes 1 and 2). These compounds demonstrated a range of selectivity for σ_2 over σ_1. As part of an effort to develop a better understanding of the structural features that drive selectivity, we have studied generated *in silico* models of both receptors. In addition, we have conducted docking studies and calculated binding energies of the exemplary compounds from our previously disclosed σ_2 ligands.

2. Materials and methods

2.1 Homology modeling

Homology modeling is a technique for creating and predicting an atomic resolution model of a target protein based on the experimentally established 3D structure of a homologous protein called the template protein. The four fundamental stages in homology modeling are (1) locating the template structure sequence, (2) matching the query sequence with the template structure sequence, (3) creating the query's model structure based on the template structure information, and (4) assessing the projected model. As a result, homology modeling may be used to predict the structure of unknown proteins, such as the human sigma 2 receptor.

The model architectures of the human sigma 2 receptor were predicted using a homology modeling approach. Maestro was used for all computational and molecular modeling of the human sigma 2 receptor (Schrödinger, LLC, 2019-1).[21] The human sigma 2 amino acid sequence, which consists of 176 residues, was retrieved from the Uniprot database (UniProt ID: Q5BJF2).[22] PSI-BLAST was used to scan the nonredundant PDB database for template identification. The X-ray crystalline structure of the *Bos taurus* sigma-2 receptor bound to Z1241145220 (PDB ID: 7M95)[23] exhibited measurable similarities to the query sequence and was therefore utilized to generate the model. Protein Data Bank was used to acquire the coordinates. The alignment of the template and the target was the initial stage. To choose the best alignment, the alignments were ordered by identities, score, positives, expectation value, and gaps, and statistically analyzed.

The Prime Module was used to create the homology models. In the model, the co-crystallized ligand Z1241145220 was retained. Using Prime functionality, loop refinement and numerous loop conformations were produced. Side-chain predictions and all-atom minimizations were used to score these conformations. The model was further optimized and minimized when the model construction calculations were completed.

2.2 Molecular docking studies

Schrödinger's Glide docking tool (Schrödinger, LLC, New York, 2019) was utilized to investigate ligand–receptor interactions. Glide is a novel method for finding favourable interactions between proteins and many ligands. As a result, Glide docking allows you to compare the binding mechanism and affinity of different ligands to the protein. In flexible docking, ligand posture refers to the location and orientation of a ligand with regard to the protein, as well as its shape. A number of hierarchical filters are used to analyze the ligand postures obtained by Glide docking. The ChemScore empirical scoring function is used by Glide. This algorithm detects the protein's and ligand's favourable hydrophobic and hydrogen-bonding interactions. Through many evaluation trials, Glide has been regarded as one of the best docking tools presently available.

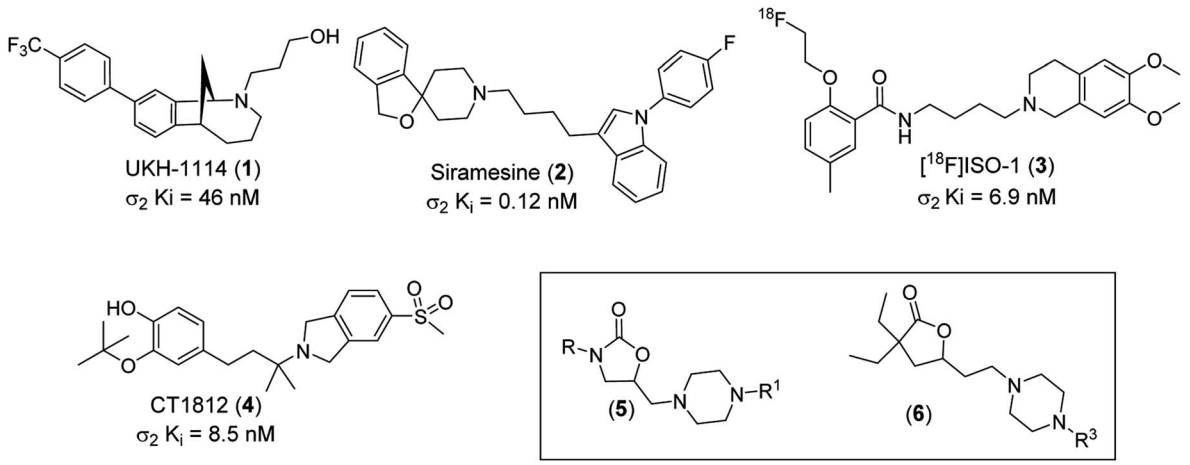

Fig. 1 Structures of UKH-1114 (**1**), Siramesine (**2**), [^{18}F]ISO-1 (**3**), CT1812 (**4**), oxazolidinone lead class (**5**) and γ-butyrolactones lead series (**6**).

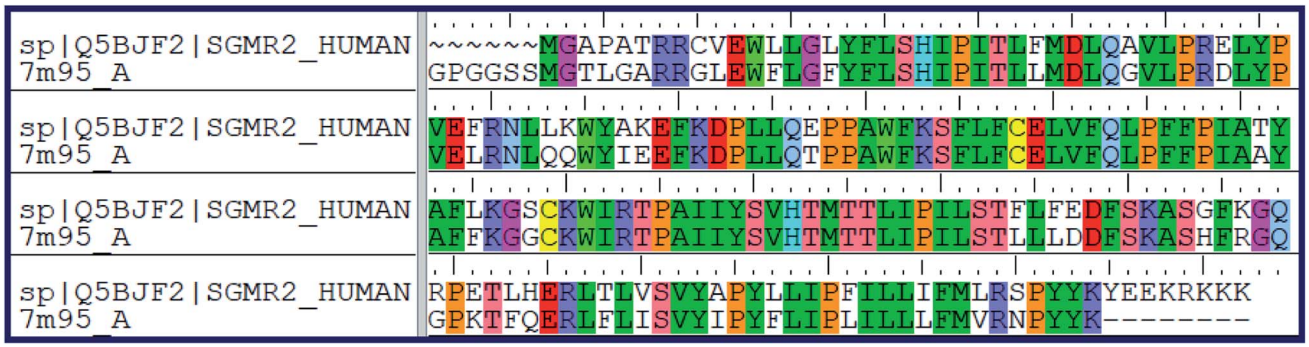

Fig. 2 Sequence alignment of sigma intracellular receptor 2 (σ_2) from *Homo sapiens* (UniProt ID:Q5BJF2) and bovine sigma-2 receptor from *Bos taurus* (PDB ID: 7M95).

2.2.1 Ligand preparation. Glide takes the ligand structure in 3D format as an input file for ligand preparation. Maestro Molecule Builder was used to create the 3D structures of all ligands. The ligand molecule is prepared for Glide docking using the Schrodinger ligand preparation product LigPrep. LigPrep (LigPrep, 2019) is a technique that refines the ligand structure *via* a series of processes. LigPrep was used to remove unnecessary structures, add hydrogens, and optimize and minimize ligand structures. Because of its enhanced parameterization and coverage, the ligand structures were reduced using the OPLS-2005 force field. Furthermore, among the force fields, the OPLS-2005 force field was selected for grid generation due to its metal handling capabilities (LigPrep, 2019). As a consequence, a single low-energy 3D structure was created with the right chiralities. LigPrep is a tool for creating high-quality 3D structures by changing chemical structures like as stereochemistry and protonation state (LigPrep, 2019). As a result, LigPrep was used to establish the protonation states of all the ligands. The protonation states of the ligand may be derived from the structure of the ligand if structural data is available. The structural data for all of the ligands is available, and the protein active site was chosen before molecular docking. As a result, the proper protonation states were assigned to the ligand binding mode.

2.2.2 Protein preparation. The RCSB Protein Data Bank was used to get the protein crystal structure of human sigma-1 receptor bound to PD144418 (PDB ID: 5HK1). Using Maestro's Protein Preparation Wizard, the human sigma-1 protein crystal structure and the modelled sigma-2 receptor were refined further. The protein's multimeric complex structure is simplified because a small number of atoms in the complex structure is preferred for computer efficiency. Except for those that have bridging connections between the protein and the ligand, all crystallographic water molecules are eliminated from the receptor molecules' 3D structure.

Customizing the protein, metal ions, and cofactors is simple using the Protein Preparation Wizard. The wizard fills in any missing residues around the protein's active site. The formal charges and ligand bond ordering were changed. Following these stages, the Impact Refinement module was used to perform restrained minimization (Impref, 2019). The revised ligand/protein/water structures were examined to guarantee the right formal charges, bond ordering, protonation states, and final changes were made to the protein structures. The receptor grid files were created using the prepared protein structures.

2.2.3 Receptor grid generation. Several distinct sets of fields were used to depict the shape and features of the grid on the receptor, providing increasingly more precise scoring of the ligand poses. One of the input files for ligand docking is the receptor grid. A prepared structure (an all-atom structure with proper bond ordering and formal charges) is required for receptor grid production, which is obtained during the protein preparation stage. A receptor grid generation panel was used to set up and produce the receptor grid for all of the proteins. The receptor structures were defined using the choices from this panel. Co-crystallized ligands were eliminated during this stage, and the location and size of the active site, which would be indicated by receptor grids, were identified. The active site of the receptor was determined using the ligands in the crystal structures. To properly address metals and a broad variety of atom types described, the force field OPLS 2005 was employed.

2.2.4 Docking studies. Glide ligand docking needed previously produced receptor grids and ligand structures built using LigPrep. By choosing XP mode on the Glide ligand docking screen, the docking was completed. The ligand docking panel's flexible docking option with default settings was chosen because it guides the docking process to build conformations internally. In terms of Glide score and docking score, Glide calculated the ligand–receptor binding affinity.

2.3 Prime MM/GBSA binding energy calculations

One of the most often used computational approaches for estimating relative binding affinities of target protein–ligand complexes is molecular mechanics with generalised born surface area (MM/GBSA). Through employing the MM/GBSA technology tools available in the Prime module of Schrodinger 2019-1, ligand-binding energies were calculated based on docking complex. The MM/GBSA calculations were performed using the protein–ligand complexes produced from the docking investigations. ΔG_{bind}, the relative binding free energy, was calculated using the following equation:

$$\Delta G_{\text{bind}} = E_{\text{complex}}\,(\text{minimized}) - [E_{\text{ligand}}(\text{unbound, minimized}) + E_{\text{receptor}}(\text{unbound, minimized})]$$

where ΔG_{bind} is the computed relative free energy that takes into account both ligand and receptor strain energy. The MM/GBSA energy of the minimized complex is E_{complex} (minimized), and E_{ligand} (unbound, minimized) is the MM/GBSA energy of the ligand after it has been removed from the complex and allowed to relax. After separating the protein from the ligand, the MM/GBSA energy of the E_{receptor} (unbound, minimized) is calculated.

3. Results and discussion

3.1 Homology modeling and binding site analysis

To the best of our knowledge, the crystal structure for sigma-2 receptor of *Homo sapiens* has not been reported yet. As a result, we used a comparative modeling approach to create a three-dimensional (3D) model for the sigma-2 receptor of *H. sapiens*. The homology model of the *H. sapiens* sigma-2 receptor was created in Schrödinger Suite 2019-1 (Schrödinger, LLC, New York, NY) using Meastro, Prime. The *H. sapiens* sigma intracellular receptor 2 query sequence was obtained from the universal protein resource (Uniprot, Entry Id: Q5BJF2). The template was chosen from the crystallographic structure of the *Bos taurus* sigma-2 receptor (PDB ID: 7M95, 2.41 resolution) with 78.4 percent sequence identity with the target. Prime homology modeling methods were used to create a 3D model of the human sigma-2 receptor. The Ramchandran plot and protein reports were used to analyze the predicted 3D structure. The sequence alignment of the sigma-2 receptor of *H. sapiens* (UniProt ID:Q5BJF2) and *Bos Taurus* (PDB ID: 7M95) is shown in Fig. 2. The homology-modeled structure of the human sigma-2 receptor and its Ramchandran plot are shown in Fig. 3 and 4. The Ramchandran plot of the human sigma-2 receptor structure revealed that >95 percent of residues are favored and allowed φ, ψ backbone conformational regions.

3.2 Molecular docking

All of the compounds were subjected to molecular docking studies in order to discover significant binding mechanisms responsible for their action on the sigma 1 and 2 receptors. Molecular docking was used to confirm the binding pose and conformation of these analogues. All of the compounds were docked into the active site of a homology-modeled sigma 2 receptor as well as the crystal structure of the sigma 1 receptor. The results of molecular docking, hydrogen bonding, and arene–arene interactions of compounds with sigma 1 and 2 receptors are shown in Tables 1 and S1.†

The initial set of compounds (**LACT1–LACT41**) comprised of a series of γ-butyrolactone analogues with a heterocyclic primary core and varied electron donating, electron withdrawing, hydrophobic, H-bond acceptor, and donor groups. When compared to the 1-diethyl lactone derivative (**LACT1**) of the γ-butyrolactone family, the 1,1-dimethyl lactone derivative (**LACT2**) demonstrates a restricted number of interactions with the active site of sigma 2 receptor. The active site residues

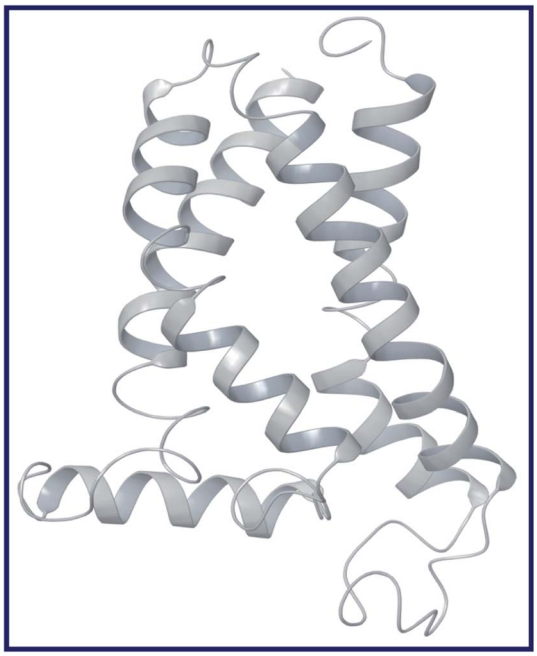

Fig. 3 Homology modelled 3D structure of human sigma intracellular receptor 2 (σ_2).

(Asp29, Glu73) of σ_2 R formed two hydrogen bonds with **LACT1**. The protonated N-atom of phenyl piperazine serves as an H-bond donor, forming an H-bond with Asp29 (d = 2.57 Å). Butyrolactone's carbonyl oxygen atom functions as an H-bond acceptor, forming an H-bond with Glu73 (d = 2.49 Å). Furthermore, piperazine's N-atom forms a Pi–cation interaction with Tyr147. **LACT1** has also exhibited a variety of hydrophobic interactions with active site residues. The phenyl ring of **LACT1** forming a Pi–Pi (arene–arene) contact with Tyr50. Furthermore, **LACT1** formed only one Pi–Pi interaction with the σ_1 R residue Tyr103 and made no H-bond interactions with it. There are fewer interactions with both σ_1 and σ_2 R for the 1,1-dimethyl lactone derivative (**LACT2**).

LACT3 with carbonyl group on its ethyl linker chain has lower docking scores towards both σ_1 & σ_2 R. **LACT4** with piperazin-2-one ring has average docking scores with fewer interactions on σ_1 & σ_2 R. **LACT5** with piperadine ring has shown good docking scores with σ_1 & σ_2 R. The N-atom of piperadine scaffold has made two strong Pi–cation interactions with the active site residues Tyr147 (d = 5.59 Å) and Tyr150 (d = 4.55 Å) of σ_2 R. Interestingly, the N-atom of piperadine also made a salt bridge with Asp29 (d = 3.07 Å) of σ_2 R. Further, the phenyl ring of **LACT5** established two Pi–Pi interactions with the active site residues Tyr103, Tyr206 of σ_1 R. In case of **LACT6**, the protonated nitrogen atom was observed at cyclohexyl connected N-atom of the piperazine ring and this N-atom interact with Asp29 *via* salt-bridge. In addition, the protonated N-atom of the piperazine ring has made a Pi–cation interaction Tyr150 of σ_2 R. Further, the protonated N-atom of the piperazine ring of **LACT6** has established an H-bond and Pi–cation interaction with Glu172 and Phe107 of σ_1 R, respectively. Compounds with electron withdrawing substituent's like CN

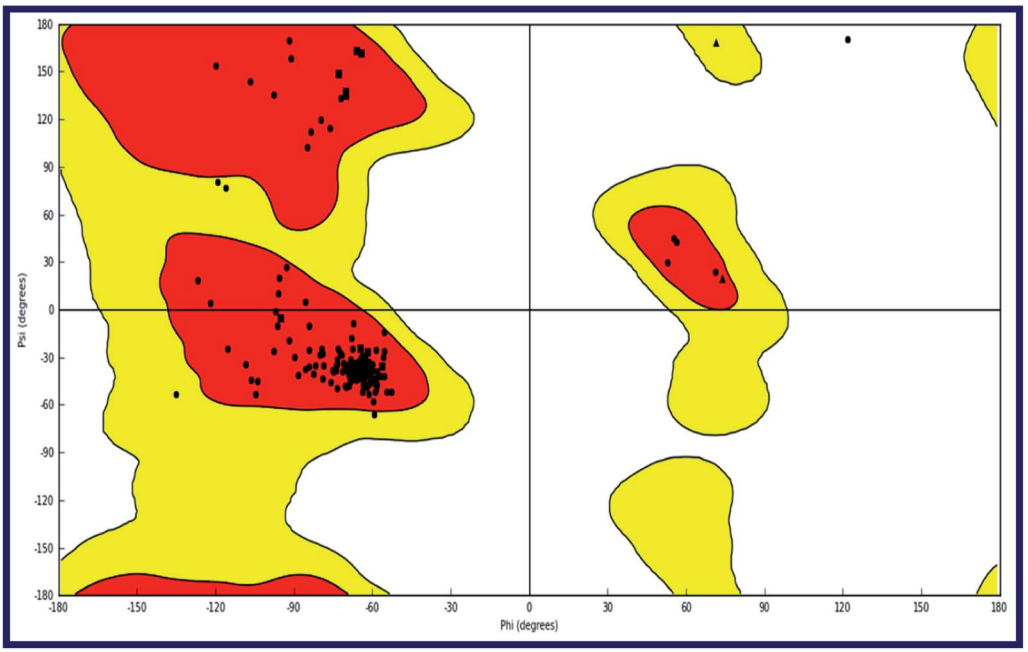

Fig. 4 Ramachandran plot for the modeled sigma intracellular receptor 2 (σ_2) of *Homo sapiens*. The plot is organized as follows: glycine, proline and all other residues are plotted as triangles, squares, and circles respectively. The red, yellow and white regions represent the favoured, allowed and the disallowed regions respectively.

Table 1 GLIDE docking score for certain γ-butyrolactone and oxazolidinone-based ligands atthe active sites of sigma intracellular receptor 1 and 2 (σ_1 and σ_2)[a]

					Interactions		
S. no	Ligand ID	Receptor name	Ki (nM)	Docking score	H- bonds	Pi–Pi stacking	Hydrophobic
1	**LACT11**	σ_1	10 000	−5.705	—	Tyr103	Val84, Trp89, Met93, Leu95, Ala98, Tyr103, Leu105, Phe107, Tyr120, Ile124, Phe133, Val162, Trp164, Met170, Ile178, Leu182, Ala185, Tyr206
		σ_2	14	−6.850	—	Tyr50	Ile24, Met28, Trp49, Tyr50, Leu59, Phe66, Phe69, Leu70, Cys72, Leu111, Ile114, Val146, Tyr147, Tyr150
2	**LACT21**	σ_1	1168	−5.681	—	—	Val84, Ala86, Trp89, Met93, Leu95, Tyr103, Leu105, Phe107, Tyr120, Ile124, Phe133, Val162, Trp164, Met170, Ile178, Leu182, Phe184, Ala185, Tyr206
		σ_2	44	−7.550	Asp29	—	Ile24, Met28, Trp49, Tyr50, Leu59, Phe66, Phe69, Leu70, Leu111, Ile114, Val146, Tyr147, Tyr150
3	**LACT22**	σ_1	195	−4.693	—	—	Val84, Trp89, Met93, Leu95, Ala98, Tyr103, Leu105, Phe107, Tyr120, Ile124, Phe133, Val152, Val162, Trp164, Met170, Ile178, Leu182, Phe184, Ala185, Leu186, Tyr206
		σ_2	5.9	−7.891	Asp29	—	Ile24, Met28, Trp49, Tyr50, Phe54, Leu59, Phe66, Leu70, Leu111, Ile114, Val146, Tyr147, Pro149, Tyr150
4	**LACT26**	σ_1	10 000	−4.983	Glu172	—	Val84, Trp89, Met93, Leu95, Ala98, Tyr103, Leu105, Tyr120, Ile124, Phe133,

Table 1 (*Contd.*)

S. no	Ligand ID	Receptor name	Ki (nM)	Docking score	Interactions		
					H- bonds	Pi–Pi stacking	Hydrophobic
							Val162, Trp164, Ile178, Leu182, Phe184, Ala185, Tyr206
		σ_2	142	−7.914	Asp29, Glu73	—	Ile24, Met28, Trp49, Tyr50, Phe54, Leu59, Phe66, Phe69, Leu70, Leu111, Ile114, Val146, Tyr147, Tyr150
5	**LACT29**	σ_1	2167	−6.486	Glu172	Tyr103, Tyr206	Val84, Trp89, Met93, Leu95, Ala98, Tyr103, Leu105, Tyr120, Ile124, Phe133, Val152, Val162, Trp164, Ile178, Leu182, Phe184, Ala185, Tyr206
		σ_2	32	−7.915	Asp29	—	Ile24, Met28, Trp49, Tyr50, Leu59, Phe66, Phe69, Leu70, Leu111, Ile114, Val146, Tyr147, Tyr150
6	**LACT35**	σ_1	125	−7.416	—	His154	Val84, Trp89, Met93, Leu95, Tyr103, Leu105, Phe107, Tyr120, Ile124, Phe133, Val162, Trp164, Ile178, Leu182, Phe184, Ala185, Leu186
		σ_2	6.1	−10.62	Asp29	—	Ile24, Met28, Tyr50, Leu59, Phe66, Phe69, Leu70, Leu111, Ile114, Val146, Tyr147, Tyr150
7	**LACT37**	σ_1	59	−7.642	—	Tyr103	Val84, Trp89, Met93, Leu95, Ala98, Tyr103, Leu105, Phe107, Tyr120, Ile124, Phe133, Val162, Trp164, Met170, Ile178, Leu182, Phe184, Ala185, Tyr206
		σ_2	2.8	−9.880	Asp29	—	Ile24, Met28, Trp49, Tyr50, Leu59, Phe66, Leu70, Leu111, Ile114, Val146, Tyr147, Tyr150
8	**LACT41**	σ_1	10 000	−7.582	Glu172	—	Val84, Trp89, Met93, Leu95, Ala98, Tyr103, Leu105, Phe107, Tyr120, Ile124, Phe133, Val162, Trp164, Ile178, Leu182, Phe184, Ala185, Tyr206
		σ_2	277	−9.292	Asp29	—	Ile24, Met28, Tyr50, Leu59, Phe66, Phe69, Leu70, Leu111, Ile114, Val146, Tyr147, Tyr150
9	**OXAZ2**	σ_1	10 000	−5.445	—	Tyr103	Val84, Trp89, Met93, Leu95, Ala98, Tyr103, Leu105, Tyr120, Ile124, Phe133, Val152, Val162, Trp164, Ile178, Leu182, Phe184, Ala185, Leu186, Tyr206
		σ_2	119	−7.113	Asp29	Tyr50	Ile24, Met28, Trp49, Tyr50, Leu59, Phe66, Leu70, Leu111, Ile114, Val146, Tyr147, Pro149, Tyr150
10	**OXAZ3**	σ_1	10 000	ND	—	—	—
		σ_2	465	−7.708	Asp29, Glu73	Phe54	Ile24, Met28, Trp49, Tyr50, Phe54, Leu59, Phe66, Phe69, Leu70, Leu111, Ile114, Val146, Tyr147, Pro149, Tyr150
11	**OXAZ4**	σ_1	10 000	ND	—	—	—
		σ_2	206	−7.627	Asp29	Phe54	Ile24, Met28, Trp49, Tyr50, Phe54, Leu59, Phe66, Leu70, Phe81, Tyr103, Leu111, Ile114, Val146, Tyr147, Pro149, Tyr150
12	**OXAZ5**	σ_1	10 000	−4.569	—	Tyr103, Tyr206	Val84, Trp89, Met93, Leu95, Ala98, Tyr103, Leu105, Tyr120, Ile124, Phe133, Val152, Val162, Trp164, Ile178, Leu182, Phe184, Ala185, Leu186, Tyr206
		σ_2	530	−6.371	—	—	Ile24, Met28, Leu46, Trp49, Tyr50, Phe54, Leu59, Phe66, Phe69, Leu70, Phe81, Tyr103, Leu111, Ile114, Val146, Tyr147, Tyr150
13	**OXAZ6**	σ_1	10 000	ND	—	—	—
		σ_2	192	−7.609	Asp29		Ile24, Met28, Trp49, Tyr50, Phe54, Leu59, Phe66, Phe69, Leu70, Leu111, Ile114, Vall46, Tyr147, Pro149, Tyr150

Table 1 (*Contd.*)

S. no	Ligand ID	Receptor name	Ki (nM)	Docking score	Interactions		
					H- bonds	Pi–Pi stacking	Hydrophobic
14	**OXAZ7**	σ_1	10 000	ND	—	—	—
		σ_2	91	−8.164	Asp29	—	Ile24, Met28, Leu46, Trp49, Tyr50, Phe54, Leu59, Phe66, Phe69, Leu70, Leu111, Ile114, Vall46, Tyr147, Tyr150
15	**OXAZ8**	σ_1	2847	−1.104	—	Trp121	Tyr120, Trp121, Ala183, Phe184, Ala187, Phe191
		σ_2	36	−10.15	—	—	Ile24, Met28, Leu46, Trp49, Tyr50, Phe54, Leu59, Phe66, Phe69, Leu70, Leu111, Ile114, Vall46, Tyr147, Tyr150
16	**OXAZ13**	σ_1	10 000	ND	—	—	—
		σ_2	49	−8.832	Asp29	Tyr150	Ile24, Met28, Trp49, Tyr50, Phe54, Leu59, Phe66, Phe69, Leu70, Leu111, Ile114, Vall46, Tyr147, Pro149, Tyr150

[a] ND# not docked at the active site.

(**LACT7**), CF_3 (**LACT8**), and Cl (**LACT9**) in the 4-position of the phenyl ring has shown good docking scores with both the σ_1 & σ_2 R. The protonated N-atom of the piperazine ring of **LACT7**, **LACT8** and **LACT9** has shown a salt-bridge and Pi–cation interaction with Asp29 and Tyr147 of σ_2 R, respectively. Additionally, an H-bond interaction was observed in between **LACT9** and Val146 of σ_2 R. Further, a salt-bridge and a Pi–cation interaction were observed for both **LACT7**, **LACT8** with Glu172 and Phe107 of σ_1 R, respectively. A Pi–Pi interaction was observed for 4-trifluoromethyl substituted phenyl ring of **LACT8**, **LACT9** with Tyr103 and Leu182 of σ_1 R, respectively.

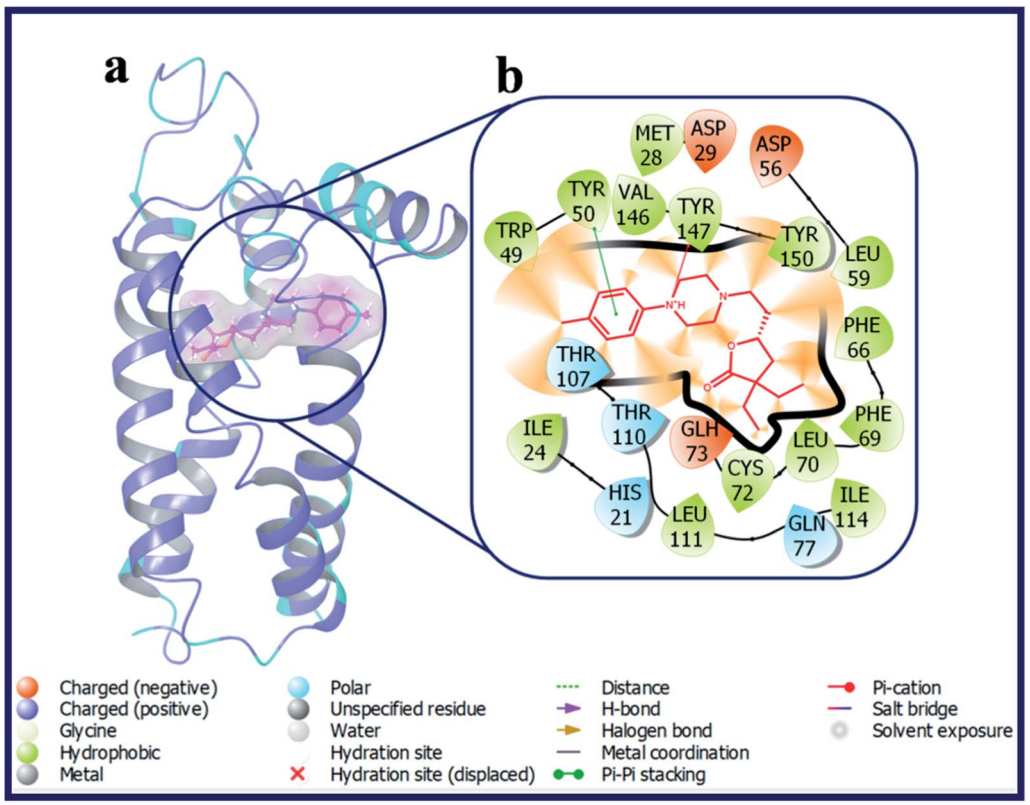

Fig. 5 (a) Docking pose of compound **LACT11** (purple colour stick) and (b) its ligand–protein interactions in the active site of modeled sigma intracellular receptor 2.

Compounds with electron donating substituent's like OMe (**LACT10**) and Me (**LACT11**) in the 4-position of the phenyl ring has shown good docking scores on σ_2 R over σ_1 R. **LACT10** established two hydrogen bonds with the active site residues (Asp29, Glu73) of σ_2 R. The protonated N-atom of phenyl piperazine has made an H-bond interaction with Asp29 and the carbonyl oxygen atom of butyrolactone shown H-bond interaction with Glu73. Further, the N-atom of piperazine is established a Pi–cation interaction with Tyr147. With respective to the σ_1 R, compound **LACT10** has formed an H-bond interaction with Glu172 and Pi–Pi interaction with His154. The detailed binding pose and protein–ligand interactions of **LACT11** with σ_2 R was depicted in Fig. 5. 4-Me substituted phenyl ring of **LACT11** established a Pi–Pi interaction with Tyr50 and N-atom of phenyl piperazine has made a Pi–cation interaction Tyr147. Further, several hydrophobic interactions were observed for **LACT11** and the active site residues of σ_2 R, which stabilizes the lodging of **LACT11** in the active pocket.

Compounds **LACT12–LACT14** include electron withdrawing substituent's at 3-position of the phenyl ring based derivatives endowed with an improved docking scores with σ_2 R if compared with the σ_1 R. The carbonyl oxygen atom of butyrolactone of **LACT12** has shown an H-bond interaction with Glu73. Further, the protonated N-atom of phenyl piperazine of both **LACT12** and **LACT13** has made a salt-bridge and a Pi–cation interaction with Asp29 and Tyr147 of σ_2 R, respectively. **LACT14** established two hydrogen bonds with the active site residues Asp29 (d = 2.29 Å), Glu73 (d = 2.3 Å) and a Pi–cation interaction with Tyr147of σ_2 R. Further, compound **LACT15** and **LACT16** with electron donating substituent's at 3-position of the phenyl ring showed almost similar docking scores on both σ_1 & σ_2 R.

Interestingly, compound **LACT17–LACT19** with electron withdrawing substituent's at 2-position of the phenyl ring showed good docking scores on σ_2 R if compared with the σ_1 R. **LACT17**, **LACT18** and **LACT19** has shared a common H-bond interaction, as well as Pi–cation interaction with the active site residues Asp29 and Tyr147 of σ_2 R, respectively. Additionally, compounds with electron donating substituent's at 2-position of the phenyl ring (**LACT20** and **LACT21**) has also shown good docking scores on σ_2 R over σ_1 R. Mounting the steric bulk in the 2-position of the phenyl ring by placing an isopropyl group (**LACT22**) improved σ_2 R selectivity. Fig. 6 displays the docking pose of **LACT22** and its ligand–protein interactions in the active site of σ_2 R. **LACT23** with 2,4-di-Me substitution on phenyl ring displayed high docking score for both σ_1 & σ_2 R. **LACT24** with 2-pyridine ring showed poor docking score at σ_2 R. In this analogue, the 2-pyridine ring was involved in the Pi–Pi stacking

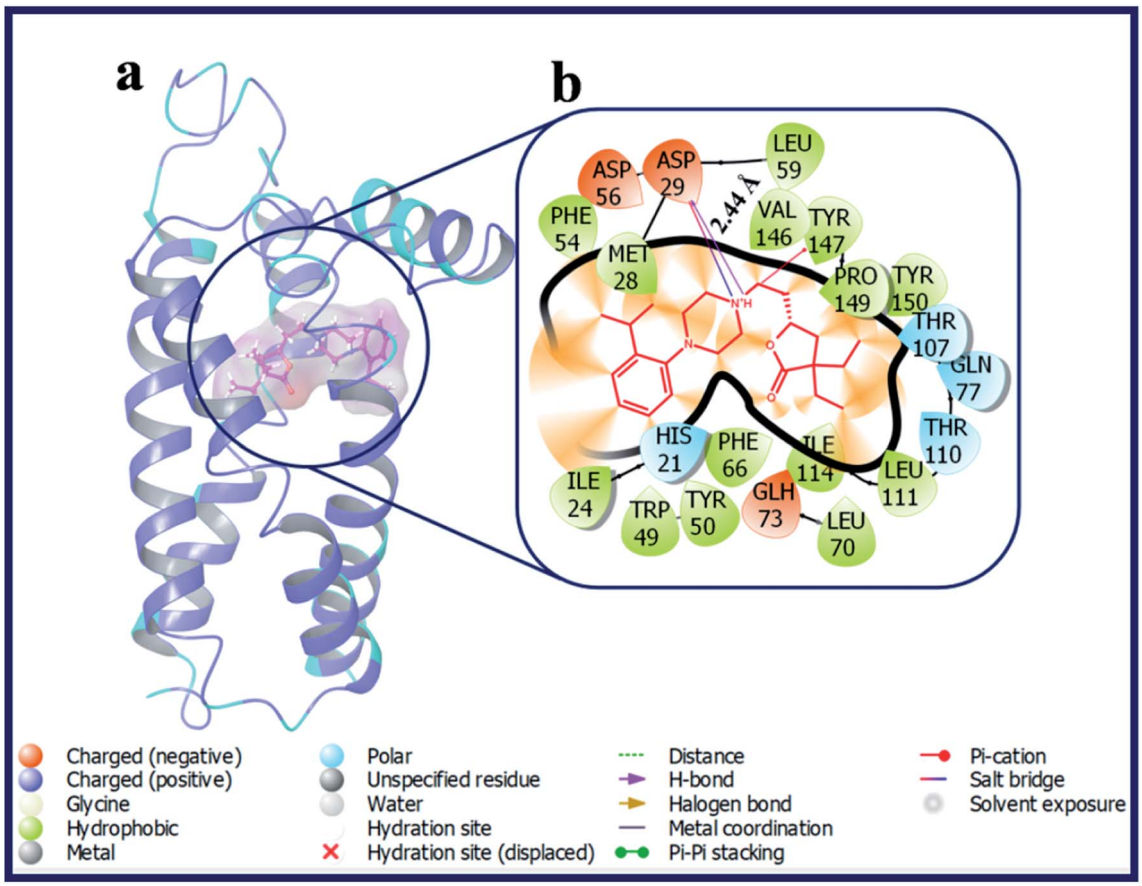

Fig. 6 (a) Docking pose of compound LACT22 (purple colour stick) and (b) its ligand–protein interactions in the active site of modeled sigma intracellular receptor 2.

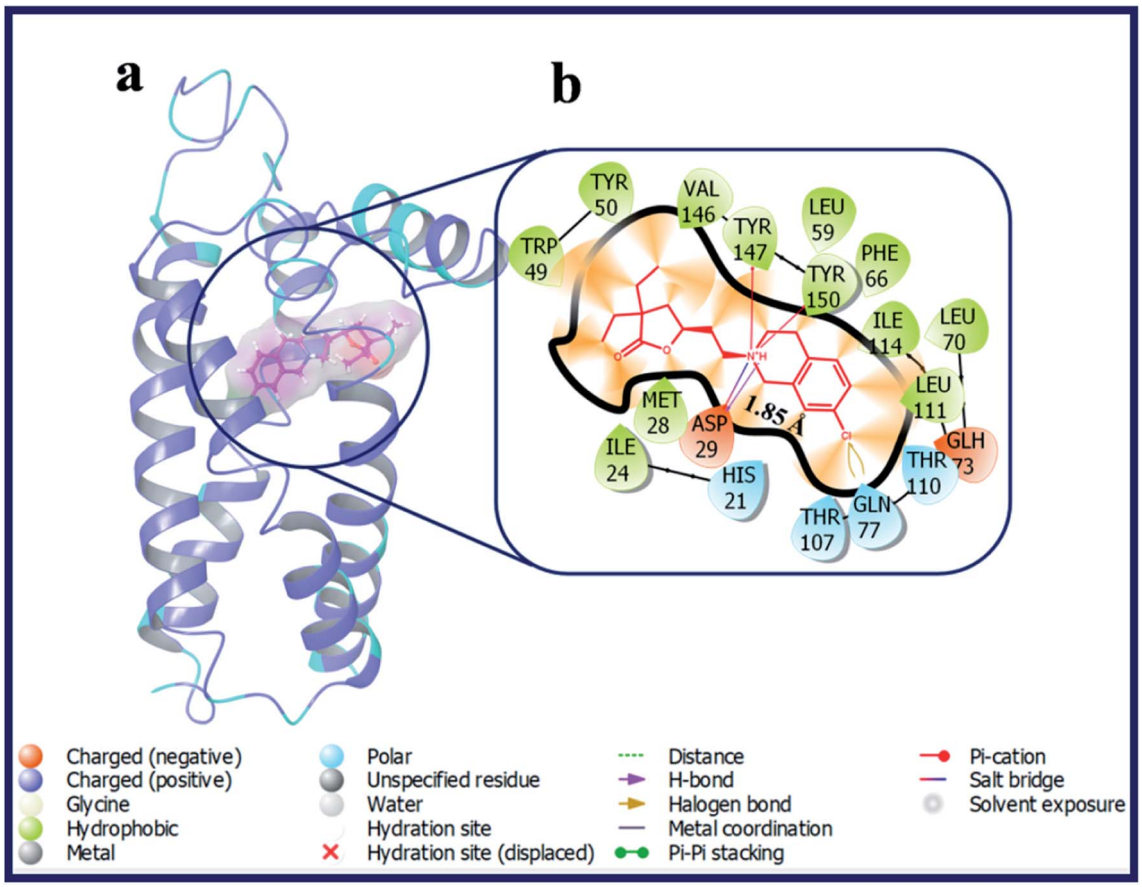

Fig. 7 (a) Docking pose of compound LACT37 (purple colour stick) and (b) its ligand–protein interactions in the active site of modeled sigma intracellular receptor 2.

interaction with Tyr50 of σ_2 R. With respective to the σ_1 R, compound **LACT24** has formed an H-bond interaction with Glu172 (d = 2.55 Å). In case of 3-pyridine ring containing analogue (**LACT25**) and 4-pyridine ring containing analogue (**LACT26**), we observed a common H-bond interactions (Asp29, Glu73) and Pi–cation interaction (Tyr147) with σ_2 R. In addition, the 3-pyridine ring of **LACT25** also involved in the Pi–Pi stacking interaction with Tyr50 of σ_2 R. Further, **LACT25** did not show any H-bond, Pi–Pi, salt-bridge and Pi–cation interactions with σ_1 R. **LACT26** exhibited an H-bond between protonated N-atom of phenyl piperazine and Glu172, and Pi–cation interaction between N-atom of 4-pyridine ring and His154 of σ_1 R.

LACT27 with linker chain length of "3C" displayed good docking score on σ_2 R over σ_1 R. The protonated N-atom of phenyl piperazine ring of **LACT27** established an H-bond, salt-bridge, Pi–cation interactions with Val146 (d = 2.56 Å), Asp29 (d = 4.68 Å), and Tyr147 (d = 4.51 Å) of σ_2 R, respectively. Compound **LACT28** include linker chain length of "4C" also shown greater docking score on σ_2 R over σ_1 R. **LACT28** established an H-bond with the active site residue Asp29 (d = 2.34 Å) and a Pi–cation interaction with Tyr147 (d = 5.06 Å) of σ_2 R. 1-Naphthyl piperazine containing γ-butyrolactone analogue (**LACT29**) displayed good docking score on σ_2 R. **LACT29** made an H-bond with the active site residue Asp29 (d = 2.13 Å) and a Pi–cation interaction with Tyr147 (d = 4.98 Å) of σ_2 R. With respective to the σ_1 R, the protonated N-atom of piperazine ring of **LACT29** has formed an H-bond interaction with Glu172 (d = 2.33 Å) and the 1-naphthyl part made two Pi–Pi interactions with the active site residues Tyr103 and Tyr206 of σ_1 R. The 4-pyrimidine ring containing γ-butyrolactone analogue (**LACT30**) displayed poor docking scores on both σ_1 and σ_2 R.

Captivatingly, compounds with prospective piperazine bioisosteres like homopiperazine analogue (**LACT31**), 2,6-diazaspiro[3.3]heptane analogue (**LACT32**), and hexahydropyrrolo [3,4-*c*]pyrrole analogue (**LACT33**) shown excellent docking scores on σ_2 R over σ_1 R. **LACT31**, **LACT32** and **LACT33** has shared a common H-bond interaction, as well as Pi–cation interaction with the active site residues Asp29 and Tyr147 of σ_2 R, respectively. Further, **LACT32** and **LACT33** have shown additional Pi–cation interaction with Tyr150 of σ_2 R. Replacing of phenyl ring in **LACT33** with 4-pyridine led to increase in number interactions with the active site residues of σ_2 R. The N-atom of 4-pyridine of **LACT34** established H-bond interaction with Gln77 (d = 2.61 Å), and also 4-pyridine formed a Pi–Pi interaction with His21 of σ_2 R. Further, **LACT34** has made H-bond interaction, as well as Pi–cation interaction with the active site residues Asp29 (d = 2.03 Å) and Tyr147 of σ_2 R, respectively.

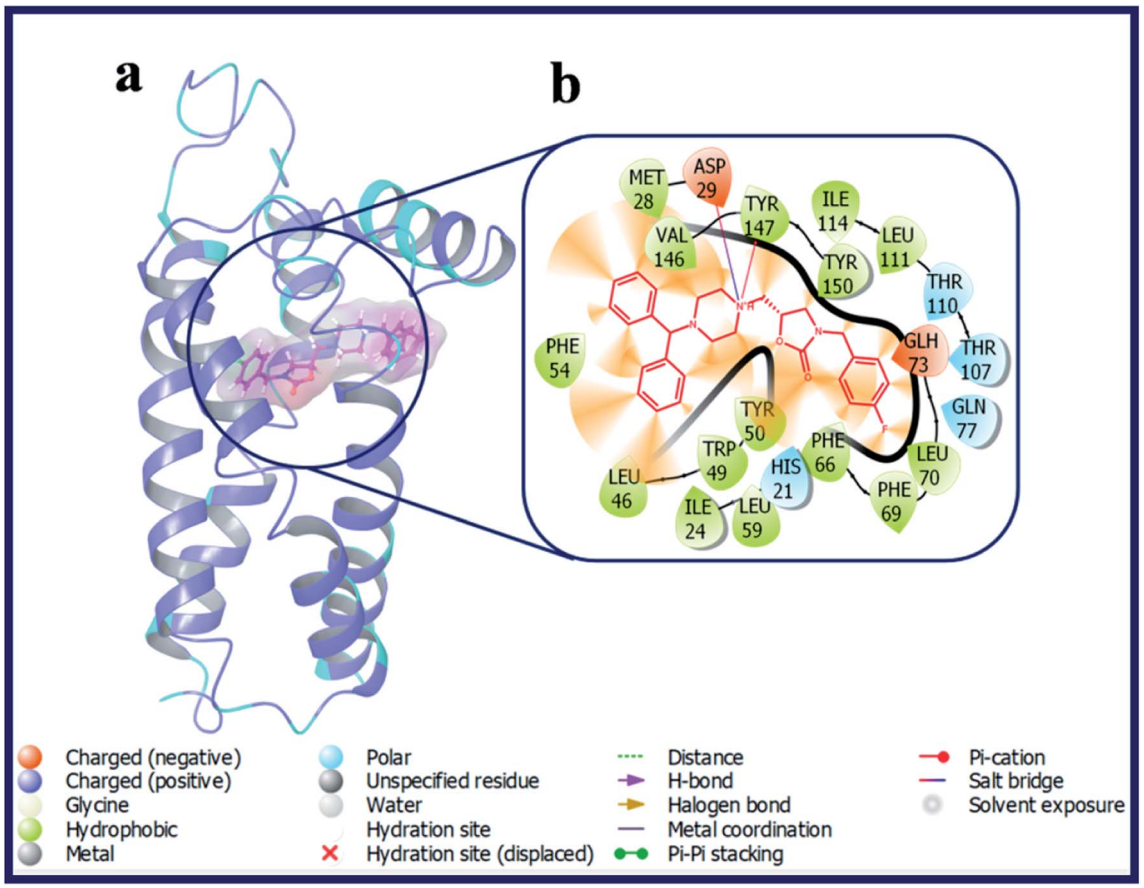

Fig. 8 (a) Docking pose of compound OXAZ8 (purple colour stick) and (b) its ligand–protein interactions in the active site of modeled sigma intracellular receptor 2.

According to our calculations, fascinatingly, compound **LACT35–LACT38** with tetrahydroisoquinoline scaffold have shown admirable docking scores with the σ_2 R. Compound **LACT35–LACT38** has shared a common H-bond interaction, as well as two Pi–cation interactions with the active site residues Asp29 and Tyr147 & Tyr150 of σ_2 R, respectively. The protonated N-atom of tetrahydroisoquinoline involved in both H-bond and Pi–cation interactions. In addition, the carbonyl oxygen atom of butyrolactone of **LACT35** is acting as H-bond acceptor and made an H-bond interaction with Gln77 ($d = 3.38$ Å). Fig. 7 illustrates the binding pose of compound **LACT37** and its ligand–protein interactions in the active site of σ_2 R. Similarly, compound **LACT39–LACT41** with pyridine type nitrogen atom in the tetrahydroisoquinoline ring also exhibited the good docking scores and interactions against both σ_1 and σ_2 R, but their actual biological K_i values are not at all potent towards the both σ_1 and σ_2 R. The *in silico* docking scores for these compounds is probably due to the close structure resemblance with that of simple tetrahydroisoquinoline scaffold containing analogues (**LACT35–LACT38**).

The second set of compounds (**OXAZ1–OXAZ17**) consisted of a series of oxazolidinone-based derivatives with a heterocyclic primary core and various electron donating, electron withdrawing, hydrophobic, H-bond acceptor, and donor groups. Within this series, compounds have various substituent's capped at amide group of oxazolidin-2-one ring. The unsubstituted oxazolidin-2-one ring containing compound **OXAZ1** displayed very poor docking scores towards both σ_1 and σ_2 R. Compounds with 3 to 6 membered cycloalkane group attachments, *i.e.* cyclopropyl (**OXAZ2**), cyclobutyl (**OXAZ3**), cyclopentyl (**OXAZ4**) and cyclohexyl (**OXAZ5**) have shown good to moderate docking scores against σ_2 R. Compound **OXAZ2** established one hydrogen bond with the active site residue (Asp29) of σ_2 R. The protonated N-atom of phenyl piperazine is acting as H-bond donor and made an H-bond interaction with Asp29 ($d = 1.80$ Å). Further, the N-atom of piperazine is established two Pi–cation interactions with Tyr147 and Tyr150. Additionally, one of the phenyl groups of benzhydryl part established a Pi–Pi interaction with Tyr50. With respective to the σ_1 R, the protonated N-atom of piperazine ring of **OXAZ2** has formed a salt-bridge with Glu172 and one of the phenyl groups of benzhydryl part established a Pi–Pi interaction with Tyr103. **OXAZ3** and **OXAZ4** have shared a common H-bond interaction, as well as Pi–cation interaction and Pi–Pi interaction with the active site residues Asp29, Tyr147 and Phe54 of σ_2 R, respectively. Further, **OXAZ3** have shown additional H-bond interaction with Glu73 of σ_2 R. On the contrary, compound **OXAZ3** and **OXAZ4** was not docked at the active site of σ_1 R. Compound **OXAZ5** exhibited a Pi–

cation interaction with Tyr147 of σ_2 R and two Pi–Pi stacking interactions with Tyr103 and Tyr206 of σ_1 R.

Compound with phenyl ring (**OXAZ6**) has showed good docking score against σ_2 R but not docked to the active site of σ_1 R. The protonated N-atom of piperazine ring of **OXAZ6** has formed an H-bond with Asp29 (d = 1.85 Å) and a Pi–cation interaction with Tyr147 of σ_2 R. Further, the phenyl group of benzhydryl part established a Pi–Pi interaction with Tyr50. **OXAZ7** with benzyl substituent showed good docking score with σ_2 R, but not docked at σ_1 R active pocket. **OXAZ8** with 4-F-benzyl substituent showed increased docking score towards σ_2 R, and poor score with σ_1 R. Better activity of **OXAZ8** with σ_2 R is probably due to the strong salt-bridge formation between N-atom of piperazine ring and Asp29 of σ_2 R. **OXAZ8** also exhibited a Pi–cation interaction with Tyr147 and Pi–Pi interaction with Phe54 of σ_2 R. In contrast, the presence of electron donating groups, such as 4-OMe (**OXAZ9**) and 4-Me (**OXAZ10**) on benzyl part led to decrease in docking scores against σ_2 R. Further, **OXAZ9** and **OXAZ10** showed very poor binding scores with σ_1 R. Fig. 8 illustrates the docking pose of compound **OXAZ8** and its ligand–protein interactions in the active site of σ_2 R. Fig. 9 displays the ligand–protein interactions for the compounds **LACT11, LACT22, LACT37** and **OXAZ8** at the active site of σ_1 R.

Compounds with a cyclohexane ring (**OXAZ11**) and tetrahydropyran ring (**OXAZ12**) also showed moderate binding with σ_2 R and very poor binding with σ_1 R. Compound **OXAZ13** with phenethyl group displayed good docking score with σ_2 R but not docked against σ_1 R active pocket. The protonated N-atom of piperazine ring of **OXAZ13** has formed an H-bond with Asp29 (d = 1.95 Å) and a Pi–cation interaction with Tyr147 of σ_2 R. Further, one of the phenyl groups of benzhydryl part established a Pi–Pi interaction with Tyr150. Further, **OXAZ14** with 4-F-phenethyl group showed poor binding with σ_2 R and σ_1 R. **OXAZ15** with 4-OMe-phenethyl group showed an H-bond interaction with Asp29 (d = 2.04 Å) and a Pi–cation interaction with Tyr147 of σ_2 R. **OXAZ16** with 4-Me-phenethyl group showed poor docking with σ_2 R and it exhibited two Pi–cation interactions with Tyr50 and Tyr147 of σ_2 R. **OXAZ17** with phenylpropyl also displayed an H-bond interaction with Asp29 (d =

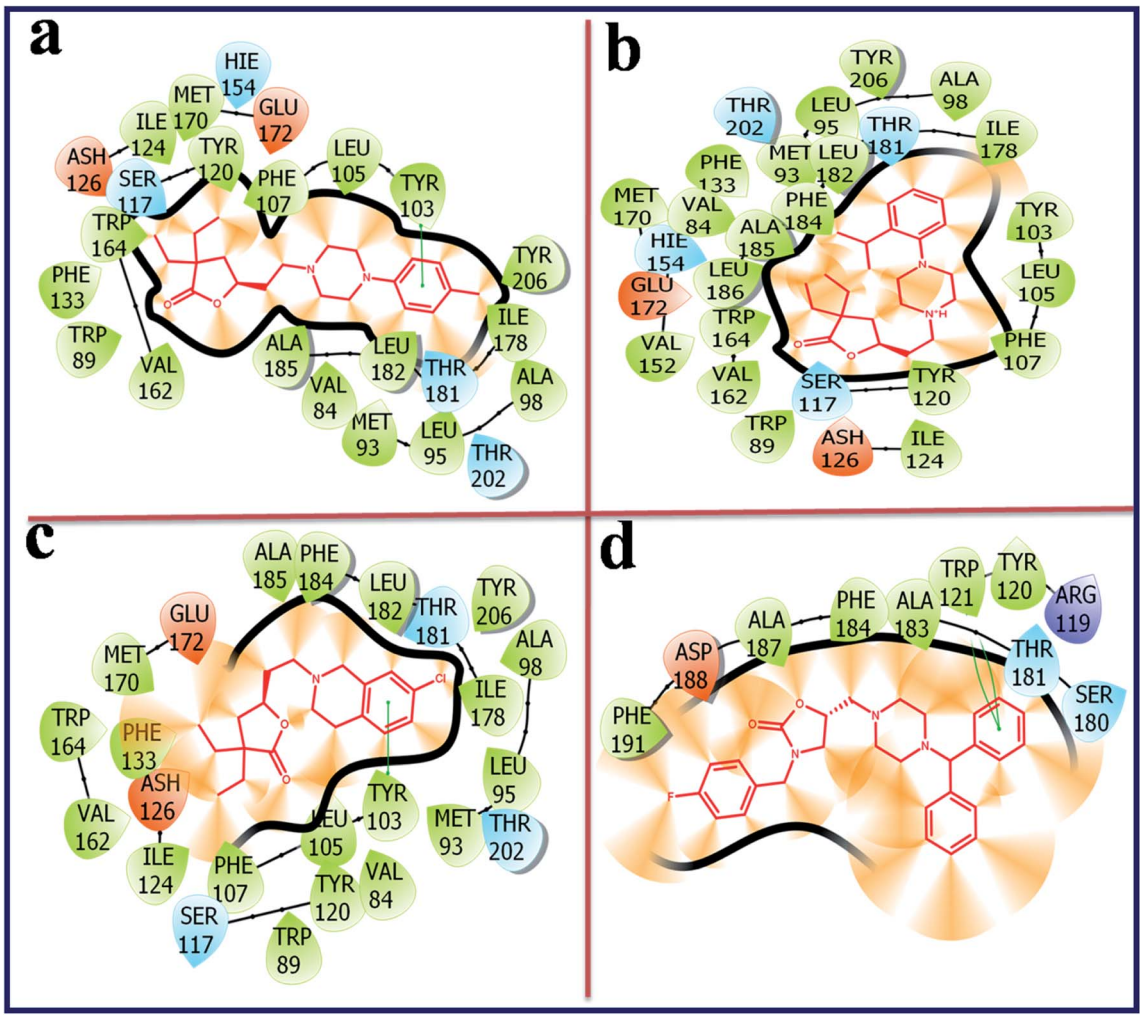

Fig. 9 Ligand–protein interaction diagram for the compound LACT11 (a), LACT22 (b), LACT37 (c) and OXAZ8 (d) at the active site of human sigma intracellular receptor 1 (PDB ID: 5HK1).

Table 2 The average ΔG_{Bind} binding free energy (kcal mol^{-1}) results from MM-GBSA calculations

S. no.	Ligand name	Receptor name	[a]ΔG_{Bind}	[b]ΔG_{Bind} Coulomb	[c]ΔG_{Bind} covalent	[d]ΔG_{Bind} H-bond	[e]ΔG_{Bind} lipo	[f]ΔG_{Bind} solv GB	[g]ΔG_{Bind} packing	[h]ΔG_{Bind} vdW
1	**LACT11**	σ_1	−72.692	−36.141	5.125	−0.110	−64.419	51.599	−0.516	−28.230
		σ_2	−84.578	−12.003	3.137	−0.042	−65.936	18.129	−0.182	−27.682
2	**LACT21**	σ_1	−70.828	−42.736	15.959	−0.490	−64.396	51.490	−0.803	−29.853
		σ_2	−100.593	−18.207	1.251	−0.751	−61.938	27.402	−0.546	−47.804
3	**LACT22**	σ_1	−82.630	−50.328	12.790	−0.742	−75.122	59.170	−0.875	−27.523
		σ_2	−93.976	−8.363	2.000	−0.564	−63.601	22.203	−0.137	−45.515
4	**LACT26**	σ_1	−62.239	2.854	7.838	−0.012	−57.765	22.889	−0.996	−37.048
		σ_2	−107.986	1.463	7.707	−0.751	−61.362	−4.223	−0.446	−50.375
5	**LACT29**	σ_1	−60.303	−1.503	16.626	−0.042	−70.189	34.138	−0.958	−38.376
		σ_2	−107.352	−12.577	2.049	−0.886	−66.412	20.676	−0.822	−49.380
6	**LACT35**	σ_1	−67.810	−2.586	6.614	−0.012	−57.729	26.364	−0.485	−39.977
		σ_2	−95.993	−15.515	5.009	−0.914	−61.545	23.716	−0.093	−46.650
7	**LACT37**	σ_1	−84.106	−4.010	6.139	−0.011	−67.887	24.824	−0.371	−42.789
		σ_2	−90.984	−22.915	9.645	−1.181	−57.791	28.408	−0.001	−47.149
8	**LACT41**	σ_1	−65.730	−0.511	5.299	−0.039	−54.189	26.266	−1.028	−41.529
		σ_2	−95.398	−14.991	5.238	−0.901	−59.999	21.977	−0.093	−46.629
9	**OXAZ2**	σ_1	−2.382	2.861	27.555	−0.037	−72.857	29.786	−3.059	13.370
		σ_2	−99.275	−3.132	8.131	−0.925	−62.137	9.443	−1.060	−49.596
10	**OXAZ3**	σ_1	—	—	—	—	—	—	—	—
		σ_2	−114.210	−12.314	3.431	−1.004	−65.374	12.458	−1.244	−50.162
11	**OXAZ4**	σ_1	—	—	—	—	—	—	—	—
		σ_2	−111.426	−12.105	2.296	−0.810	−63.686	17.158	−1.379	−52.898
12	**OXAZ5**	σ_1	−2.018	4.574	32.115	−0.004	−81.300	32.921	−2.689	12.365
		σ_2	−120.283	−14.860	9.246	−0.038	−68.995	15.282	−0.186	−60.732
13	**OXAZ6**	σ_1	—	—	—	—	—	—	—	—
		σ_2	−97.551	−5.157	9.508	−0.711	−57.962	11.774	−0.987	−54.016
14	**OXAZ7**	σ_1	—	—	—	—	—	—	—	—
		σ_2	−103.179	−3.886	5.441	−0.478	−61.168	11.805	−0.022	−54.871
15	**OXAZ8**	σ_1	−45.625	−4.248	3.120	−0.224	−26.243	16.691	−0.444	−34.277
		σ_2	−103.320	−10.931	10.362	−0.415	−63.127	15.993	−0.220	−54.983
16	**OXAZ13**	σ_1	—	—	—	—	—	—	—	—
		σ_2	−104.800	−11.373	5.611	−0.774	−63.712	18.488	−1.227	−51.812
17	[i]**PD144418**	σ_1	−92.772	−52.669	4.382	−0.784	−52.904	56.883	−0.219	−47.460
18	[j]**Z1241145220**	σ_2	−92.982	−23.867	4.044	−1.290	−51.544	29.613	−0.276	−49.662

[a] Free energy of binding. [b] Coulomb energy. [c] Covalent energy (internal energy). [d] Hydrogen bonding correction. [e] Lipophilic energy. [f] Electrostatic solvation energy. [g] Pi–pi packing correction. [h] van der Waals energy. [i] PD144418 = 3-(4-methylphenyl)-5-(1-propyl-3,6-dihydro-2*H*-pyridin-5-yl)-1,2-oxazole. [j] Z1241145220 = 3-[1-(3-phenylpropyl)-1,2,3,6-tetrahydropyridin-4-yl]-1*H*-pyrrolo[2,3-*b*]pyridine.

2.34 Å) and a Pi–cation interaction with Tyr147 of σ_2 R. Further, compound **OXAZ15**, **OXAZ16** and **OXAZ17** showed very poor binding score with the active site of σ_1 R.

3.3 Prime MM/GBSA binding energy calculations

To further authenticate the binding affinity of docked γ-butyrolactone and oxazolidinone-based ligands at the active sites of the sigma 1 and sigma 2 receptors, binding free energy was calculated using the molecular mechanics generalised born surface area (MM-GBSA) approach available in the Prime module. Table 2 summarizes the binding energies of certain γ-butyrolactone and oxazolidinone-based ligands based on biological K_i values and the σ_2/σ_1 ratio.

The estimated binding free energy of docked poses of molecules with σ_1 receptor ranged from −2.018 to −84.106 kcal mol^{-1}, whereas the BFG score for the σ_2 receptor ranged from −84.578 to −114.210 kcal mol^{-1}. The study shows that produced chemicals bind to the σ_2 receptor at a higher rate than those that bind to the σ_1 receptor. The docking complexes for the chemicals **OXAZ3**, **OXAZ4**, **OXAZ6**, **OXAZ7**, and **OXAZ13** were not identified. So, their binding energies were assumed to be 0 kcal mol^{-1}. The compound **OXAZ3** with the σ_2 receptor has the greatest BFG score of around −114.210 kcal mol^{-1}. The van der Waal energy (G_{vdW} = −50.162 kcal mol^{-1}) and lipophilic energy (G_{lipo} = −65.374 kcal mol^{-1}) terms are the major contributors to **OXAZ3** binding activity in the active pocket of the σ_2 receptor, while coulombic energy (G_{cou} = −12.314 kcal mol^{-1}) moderately favours ligand binding, according to this study. Furthermore, the ligand's binding activity inside the active site of the σ_2 receptor is deemed unfavourable due to covalent energy and electrostatic solvation energy terms. Nonetheless, when compared to the σ_1 receptor, the compounds had lower BFG, van der Waal energy, lipophilic energy, and coulombic energy. The results show that the produced compounds had a higher affinity for the σ_2 receptor than the σ_1 receptor.

4. Conclusion

In this work, essential components responsible for the binding process between the σ_2 receptor and its ligands were identified utilizing molecular docking and MM/GBSA binding energy calculations. Molecular docking study provides a useful prediction of structural features for certain series of compounds belonging to γ-butyrolactone and oxazolidinones to bind at the active sites of σ_1 and σ_2 receptor. A 3D homology model for the σ_2 receptor was built to perform the modeling studies. The Ramchandran plot examination was conducted to assess the correctness of modeled σ_2 receptor. The putative binding site on the modeled σ_2 receptor was identified using SiteMap analysis. In this present work, a total of 58 compounds have been used. The molecules were docked into both the active site of a homology-modeled σ_2 receptor and the crystal structure of the σ_1 receptor. The structural features required for ligand binding to σ_1 and σ_2 receptors were studied in 2D and 3D. With the σ_2 receptor, the ligands showed higher BFG, van der Waal energy, lipophilic energy, and coulombic energy. The top-ranked molecules, according to the above study, had much more interactions and binding energy for the σ_2 receptor than the σ_1 receptor. Thus, the present study provides an understanding of the specific pharmacophoric features and interactions of ligands that are responsible for σ_2 selectivity over σ_1 receptor. Future research on these molecules might lead to the discovery of novel and potential selective σ_2 ligands.

Conflicts of interest

The authors declare no conflicts of interest.

Acknowledgements

The authors (DKS, ABS) would like to acknowledge Vignan Pharmacy College, Vadlamudi, Andhra Pradesh, India. RRB would like to thank Deanship of Graduate Studies and Research, Ajman University, UAE for their support in providing partial assistance in article processing charges of this manuscript. DC and BB would like to extend their thanks to Dean's office at Temple School of Pharmacy for their support in the preparation of this manuscript.

References

1 W. R. Martin, C. E. Eades, J. A. Thompson and R. E. Huppler, The effects of morphine and nalorphine-like drugs in the non-dependent and morphine-dependent chronic spinal dog, *J. Pharmacol. Exp. Ther.*, 1976, **197**(3), 517–532.

2 T. P. Su, Evidence for sigma opioid receptor: binding of [3H] SKF-10047 to etorphine inaccessible sites in guinea-pig brain, *J. Pharmacol. Exp. Ther.*, 1982, **223**(2), 284–290, DOI: 10.1007/s00044-020-02574-9.

3 W. D. Bowen, B. R. de Costa, S. B. Hellewell, J. M. Walker and K. C. Rice, [3H]-(+)-Pentazocine: a potent and highly selective benzomorphan-based probe for sigma-1 receptors, *Mol. Neuropharmacol.*, 1993, **3**, 117–126.

4 H. R. Schmidt, S. Zheng, E. Guripinar, A. Koehl, A. Manglik and A. C. Kruse, Crystal structure of the human σ1 receptor, *Nature*, 2016, **532**(7600), 527–530, DOI: 10.1038/nature17391.

5 A. Alon, H. R. Schmidt, M. D. Wood, J. J. Sahn, S. F. Martin and A. C. Krusea, Identification of the gene that codes for the σ2 receptor, *Proc. Natl. Acad. Sci. U. S. A.*, 2017, **114**(27), 7160–7165, DOI: 10.1073/pnas.1705154114.

6 A. Alon, J. Lyu, J. M. Braz, T. A. Tummino, V. Craik, M. J. O'Meara, C. M. Webb, D. S. Radchenko, Y. S. Moroz, X. P. Huang, Y. Liu, B. L. Roth, J. J. Irwin, A. I. Basbaum, B. K. Shoichet and A. C. Kruse, Structures of the σ2 receptor enable docking for bioactive ligand discovery, *Nature*, 2021, **600**(7890), 759–764, DOI: 10.1038/s41586-021-04175-x.

7 F. Bartz, L. Kern, D. Erz, M. Zhu, D. Gilbert, T. Meinhof, U. Wirkner, H. Erfle, M. Muckenthaler, R. Pepperkok and H. Runz, Identification of cholesterol-regulating genes by targeted RNAi screening, *Cell Metab.*, 2009, **10**(1), 63–75, DOI: 10.1016/j.cmet.2009.05.009.

8 L. Guo and X. Zhen, Sigma-2 receptor ligands: neurobiological effects, *Curr. Med. Chem.*, 2015, **22**(8), 989–1003, DOI: 10.2174/0929867322666150114163607.

9 (*a*) B. Yi, J. J. Sahn, P. M. Ardestani, A. K. Evans, L. L. Scott, J. Z. Chan, S. Iyer, A. Crisp, G. Zuniga, J. T. Pierce, S. F. Martin and M. Shamloo, Small molecule modulator of sigma 2 receptor is neuroprotective and reduces cognitive deficits and neuroinflammation in experimental models of Alzheimer's disease, *J. Neurochem.*, 2017, **140**(4), 561–575, DOI: 10.1111/jnc.13917; (*b*) N. J. Izzo, A. Staniszewski, L. To, M. Fa, A. F. Teich, F. Saeed, H. Wostein, T. Walko, A. Vaswani, M. Wardius, Z. Syed, J. Ravenscroft, K. Mozzoni, C. Silky, C. Rehak, R. Yurko, P. Finn, G. Look, G. Rishton, H. Safferstein, M. Miller, C. Johanson, E. Stopa, M. Windisch, B. Hutter-Paier, M. Shamloo, O. Arancio, H. LeVine and S. M. Catalano, Alzheimer's therapeutics targeting amyloid beta 1−42 oligomers I: Abeta 42 oligomer binding to specific neuronal receptors is displaced by drug candidates that improve cognitive deficits, *PLoS One*, 2014, **9**(11), e111898, DOI: 10.1371/journal.pone.0111898; (*c*) N. J. Izzo, J. Xu, C. Zeng, M. J. Kirk, K. Mozzoni, C. Silky, C. Rehak, R. Yurko, G. Look, G. Rishton, H. Safferstein, C. Cruchaga, A. Goate, M. A. Cahill, O. Arancio, R. H. Mach, R. Craven, E. Head, H. LeVine, T. L. Spires-Jones and S. M. Catalano, Alzheimer's therapeutics targeting amyloid beta 1−42 oligomers II: Sigma-2/PGRMC1 receptors mediate Abeta 42 oligomer binding and synaptotoxicity, *PLoS One*, 2014, **9**(11), e111899, DOI: 10.1371/journal.pone.0111899.

10 J. J. Sahn, G. L. Mejia, P. R. Ray, S. F. Martin and T. J. Price, Sigma 2 receptor/Tmem97 agonists produce long lasting antineuropathic pain effects in mice, *ACS Chem. Neurosci.*, 2017, **8**(8), 1801–1811, DOI: 10.1021/acschemneuro.7b00200.

11 E. Vazquez-Rosa, M. R. Watson, J. J. Sahn, T. R. Hodges, R. E. Schroeder, C. J. Cintron-Perez, M. K. Shin, T. C. Yin, J. L. Emery, S. F. Martin, D. J. Liebl and A. A. Pieper,

Neuroprotective Efficacy of a Sigma 2 Receptor/TMEM97 Modulator (DKR-1677) after Traumatic Brain Injury, *ACS Chem. Neurosci.*, 2019, **10**(3), 1595–1602, DOI: 10.1021/acschemneuro.8b00543.

12 D. Ebrahimi-Fakhar, L. Wahlster, F. Bartz, J. Werenbeck-Ueding, M. Praggastis, J. Zhang, B. Joggerst-Thomalla, S. Theiss, D. Grimm, D. S. Ory and H. Runz, Reduction of TMEM97 increases NPC1 protein levels and restores cholesterol trafficking in Niemann-pick type C1 disease cells, *Hum. Mol. Genet.*, 2016, **25**(16), 3588–3599, DOI: 10.1093/hmg/ddw204.

13 (*a*) B. J. Vilner, C. S. John and W. D. Bowen, Sigma-1 and Sigma-2 receptors are expressed in a wide variety of human and rodent tumor cell lines, *Cancer Res.*, 1995, **55**(2), 408–413; (*b*) G. Asong, X. Y. Zhu, B. Bricker, T. Andey, F. Amissah, N. Lamango and S. Y. Ablordeppey, New analogs of SYA013 as sigma-2 ligands with anticancer activity, *Bioorg. Med. Chem.*, 2019, **27**(12), 2629–2636, DOI: 10.1016/j.bmc.2019.04.012.

14 (*a*) J. J. Sahn, G. L. Mejia, P. R. Ray, S. F. Martin and T. J. Price, Sigma 2 Receptor/Tmem97 Agonists Produce Long Lasting Antineuropathic Pain Effects in Mice, *ACS Chem. Neurosci.*, 2017, **8**(8), 1801–1811, DOI: 10.1021/acschemneuro.7b00200; (*b*) W. D. Bowen, C. M. Bertha, B. J. Vilner and K. C. Rice, Antinociceptive CB-64D and CB-184: ligands with high σ2 receptor affinity and subtype selectivity, *Eur. J. Pharmacol.*, 1995, **278**(3), 257–260, DOI: 10.1016/0014-2999(95)00176-L.

15 J. Perregaard, E. K. Moltzen, E. Meier and C. Sánchez, Sigma ligands with subnanomolar affinity and preference for the sigma 2 binding site. 1. 3-(omega-aminoalkyl)-1H-indoles, *J. Med. Chem.*, 1995, **38**(11), 1998–2008, DOI: 10.1021/jm00011a019.

16 E. S. McDonald, R. K. Doot, A. J. Young, E. K. Schubert, J. Tchou, D. A. Pryma, M. D. Farwell, A. Nayak, A. Ziober, M. D. Feldman, A. DeMichele, A. S. Clark, P. D. Shah, H. Lee, S. D. Carlin, R. H. Mach and D. A. Mankoff, Breast Cancer 18F-ISO-1 Uptake as a Marker of Proliferation Status, *J. Nucl. Med.*, 2020, **61**(5), 665–670, DOI: 10.2967/jnumed.119.232363.

17 G. M. Rishton, G. C. Look, Z. J. Ni, J. Zhang, Y. Wang, Y. Huang, X. Wu, N. J. Izzo, K. M. LaBarbera, C. S. Limegrover, C. Rehak, R. Yurko and S. M. Catalano, Discovery of Investigational Drug CT1812, an Antagonist of the Sigma-2 Receptor Complex for Alzheimer's Disease, *ACS Med. Chem. Lett.*, 2021, **12**(9), 1389–1395, DOI: 10.1021/acsmedchemlett.1c00048.

18 B. E. Blass, R. Gao, K. M. Blattner, J. C. Gordon, D. A. Pippin and D. J. Canney, Synthesis and evaluation of novel, selective, functionalized γ-butyrolactones as sigma-2 ligands, *Med. Chem. Res.*, 2022, **31**(2), 337–349, DOI: 10.1007/s00044-021-02831-5.

19 B. E. Blass, R. R. Bhandare and D. J. Canney, Discovery of oxazolidinone-based heterocycles as subtype selective sigma-2 ligands, *Med. Chem. Res.*, 2022, **31**(3), 416–425, DOI: 10.1007/s00044-022-02848-4.

20 B. E. Blass, R. Gao, K. M. Blattner, J. C. Gordon, D. A. Pippin and D. J. Canney, Design, synthesis, and evaluation of novel, selective γ-butyrolactones sigma-2 ligands, *Med. Chem. Res.*, 2021, **30**(9), 1713–1727, DOI: 10.1007/s00044-021-02771-0.

21 *Schrödinger Release 2019-1*, Maestro, Schrödinger, LLC, New York, NY, 2019.

22 https://www.uniprot.org/uniprot/Q5BJF2.

23 A. Alon, J. Lyu, J. M. Braz, T. A. Tummino, V. Craik, M. J. O'Meara, C. M. Webb, D. S. Radchenko, Y. S. Moroz, X. P. Huang, Y. Liu, B. L. Roth, J. J. Irwin, A. I. Basbaum, B. K. Shoichet and A. C. Kruse, Structures of the sigma 2 receptor enable docking for bioactive ligand discovery, *Nature*, 2021, **600**, 759–764, DOI: 10.1038/s41586-021-04175-x.